PHOTONICS Research

Sequential trapping of single nanoparticles using a gold plasmonic nanohole array

Xue Han,[1] Viet Giang Truong,[1,*] Prince Sunil Thomas,[1,3] and Síle Nic Chormaic[1,2]

[1]Light-Matter Interactions Unit, Okinawa Institute of Science and Technology Graduate University, Onna, Okinawa 904-0495, Japan
[2]Université Grenoble Alpes, CNRS, Grenoble INP, Institut Néel, 38000 Grenoble, France
[3]Current address: Advanced Optical Imaging Group, School of Physics, University College Dublin, Ireland
*Corresponding author: v.g.truong@oist.jp

Received 4 May 2018; revised 2 August 2018; accepted 2 August 2018; posted 28 August 2018 (Doc. ID 330950); published 1 October 2018

We have used a gold nanohole array to trap single polystyrene nanoparticles, with a mean diameter of 30 nm, into separated hot spots located at connecting nanoslot regions. A high trap stiffness of approximately 0.85 fN/(nm · mW) at a low-incident laser intensity of ~0.51 mW/μm^2 at 980 nm was obtained. The experimental results were compared to the simulated trapping force, and a reasonable match was achieved. This plasmonic array is useful for lab-on-a-chip applications and has particular appeal for trapping multiple nanoparticles with predefined separations or arranged in patterns in order to study interactions between them. © 2018 Chinese Laser Press

OCIS codes: (240.6680) Surface plasmons; (170.4520) Optical confinement and manipulation; (350.4855) Optical tweezers or optical manipulation.

https://doi.org/10.1364/PRJ.6.000981

1. INTRODUCTION

Plasmonic tweezers [1], based on nanostructures fabricated on metallic thin films, can overcome the diffraction limit, which inhibits the wide use of conventional, single-beam, gradient force optical tweezers in nanoparticle trapping [2]. With plasmonic tweezers, an incident beam can be confined to nanoscale dimensions via the excitation of localized surface plasmon polaritons (LSPPs) in nanostructures [3,4]. For small particles (0.5–1.5 μm), cluster or single particle trapping and manipulation have been achieved using plasmonic tweezers based on arrays of nanostructures [5–7]. A single nanoparticle has been successfully trapped using a single nanostructure, such as a bow-tie nanoaperture or a double nanohole [8,9]. Aside from the more standard polystyrene (PS) and silica particles, quantum dots [10], single proteins [11], and *Escherichia coli* bacteria [12] have also been trapped by plasmonic tweezers [13].

For some applications, it is more attractive to trap nanoparticles with specific selectivity, e.g., size, weight, and refractive index, rather than being limited to single-particle trapping. For example, in nanobiotechnology, advanced techniques are often needed, such as for the immersion of metal nanoprobes into nanomolecule complexes [14], selection of particles of different sizes [6], or multisensing in microarrays [15]. The motivation behind selective trapping of multiple nano-objects in a microarray system is the desire to develop a compact device that could have considerable impact in biomedicine, pharmacology, and environmental safety [16,17].

In this work, first, we present our design of a plasmonic tweezers array and a simulation of the optical forces acting on trapped nanoparticles based on Maxwell stress tensor method. Next, we demonstrate trapping of single PS nanoparticles, with a mean diameter of 30 nm, in multiple trapping sites of the plasmonic nanohole array using low-incident laser intensities (approximately 0.64 mW/μm^2 at the maximum value). Here, we emphasize one feature of this array, i.e., the sequential trapping and detection of single nanoparticles. While several proposals exist on trapping nanoparticles with a plasmonic array [18,19], to our knowledge, this is the first demonstration of trapping multiple nanoparticles at distant hot spots of a plasmonic array device. This plasmonic tweezer has huge potential as a lab-on-a-chip in order to trap nanoscale particles at distinct hot spots and to study interactions between nearby particles. It may be extended towards applications such as highly sensitive kinetic detection of trace amounts of analytes (toxin, drug, etc.) in a complex solution.

2. NANOARRAY FABRICATION AND CHARACTERIZATION

An array of nanoholes containing 10 × 15 identical units was fabricated on a gold (50 nm thickness)-coated coverslip (PHASIS Geneva, BioNano) using focused ion beam (FIB) milling, details of which are contained elsewhere [20]. The connecting nanoslots were fabricated along the x direction, leading to nanotips along the y direction. A scanning electron microscope (SEM) image of an array is shown in Fig. 1(a). A higher magnification SEM image of a single pair of double nanoholes, fabricated using the same conditions and located at 3 μm from

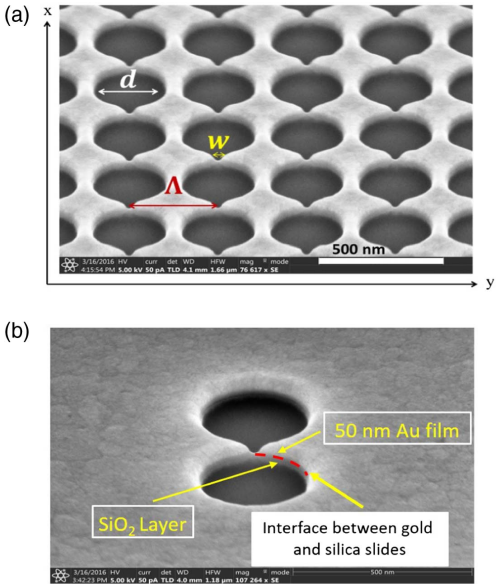

Fig. 1. (a) SEM image of a fabricated nanohole array. The nanoslot is designed to connect the nanoholes of diameter d, along the x direction, and w is the width of the nanoslot, i.e., the separation between the nanotips. Λ is the period for both the x and y directions; (b) higher magnification image of double nanoholes, fabricated using the same conditions as for (a) and located 3 μm from the edge of the array. The z direction is pointing into the plane of the paper.

the edge of the array, is shown in Fig. 1(b). The image shows slight overetching of approximately 30 nm into the silica slide. On average, the diameter of the fabricated nanoholes is $d = 277.4 \pm 8.1$ nm, the width of the nanoslots is $w = 44.4 \pm 4.3$ nm, and the period of the array is $\Lambda = 359.1 \pm 3.0$ nm in both the x and y directions. A longitudinally polarized incident laser beam (i.e., with the electric field polarized along the y direction) can be used to excite the gap mode in the nanoslot areas.

As a first step, we used COMSOL Multiphysics to evaluate the transmission spectra and optical forces on nanoparticles via a nanohole array with parameters similar to those we have fabricated. In the simulations, we also use a structure that is on a 50 nm gold film. The top layer is a glass substrate of 400 nm thickness, and the bottom layer is water of 350 nm thickness. The unit area for simulations is 360 nm × 360 nm, and the Floquet periodic condition was used to simulate the array. Perfectly matched layers (PMLs) of 100 nm thickness were used for both the glass substrate (top) and the water (bottom). This value was chosen to ensure that all reflected and scattered light was absorbed so as to eliminate any interference effects in the simulations. A plane wave at normal incidence passes from the glass substrate to the nanohole. We chose the electric field of the incident light to be polarized along the y direction to excite the LSPPs located at the nanoslots. An incident laser intensity of 100 mW/μm^2 was used in all simulations, and the nanohole pattern was cut into the glass substrate at a depth of 30 nm to provide a short distance over which the nanoparticle can move close to the gold/glass interface.

Extinction spectra were used as an indicator of the resonance peak position for the nanohole array. Figures 2(a) and 2(b)

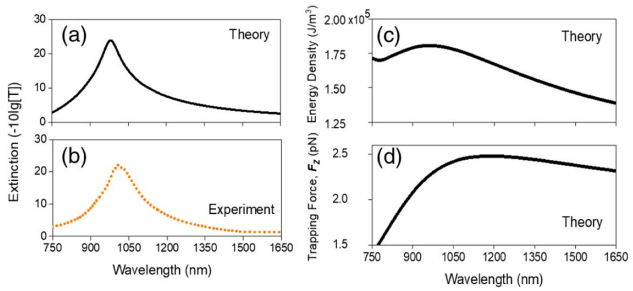

Fig. 2. (a) Simulated and (b) experimental extinction curves extracted from the transmission spectra; (c) energy density from the highest near-field confined area and (d) trapping force along the z direction as a function of wavelength.

show the theoretical and experimental extinction curves extracted from the transmission spectra. A microspectrophotometer (MSP) was used to measure the transmission through the fabricated array surrounded by water. The experimentally measured extinction peak at $\lambda = 1010$ nm differs from the theoretical one of $\lambda = 980$ nm. This could be due to imperfections during the fabrication process that cause the edges of the features in the structure to be rounded, whereas they are treated as sharp in simulations [21]. The plots in Figs. 2(c) and 2(d) represent the simulated energy density at the strongest near-field confined area and the optical force acting on a 30 nm PS bead as a function of laser wavelength, respectively. As expected, the observed absorption peak at 960 nm in the energy density curve is close to the theoretical extinction peak at ~980 nm.

In Fig. 2(d), the optical force, F_z, arising from 100 mW/μm^2 incident laser intensity, rapidly increases from 1.4 pN at 750 nm to 2.5 pN at 1125 nm and then decreases gradually. Based on the theoretical prediction and the extinction spectrum measurement, we subsequently chose incident light with a wavelength range between 940 and 980 nm to experimentally demonstrate trapping of 30 nm PS nanoparticles, details of which are contained in Section 3. It is worth noting that, for the simulation of the force, the particle was localized at the equilibrium position.

We have also compared the simulated extinction spectra both with and without a 30 nm PS particle. When a particle is trapped in the nanoslot areas, the resonance extinction peak is redshifted by ~3 nm (figure not shown), corresponding to an increase in incident light transmission of about 1% at the resonant 980 nm or 10% at the off-resonant 940 nm. The total time-independent electromagnetic force acting on the particle can be calculated from the integration of the Maxwell stress tensor over the surface of the particle [18], and is given by

$$\boldsymbol{F} = \oint_s (\langle \boldsymbol{T}_M \rangle \cdot \boldsymbol{n}_s) \mathrm{d}S, \tag{1}$$

where $\boldsymbol{n}_s$ is a normal vector pointing away from the surface S and $\langle \boldsymbol{T}_M \rangle$ is the time-independent Maxwell stress tensor. The trapping potential, $U(r)$, resulting from the optical forces determines the stability of the near-field trap and can be obtained from

$$U(r) = \int_{\infty}^{r} F(r') \mathrm{d}r', \tag{2}$$

where r is the position of the nanoparticle.

In the following, we present simulation results for the optical force and the trapping potential at the resonant wavelength, $\lambda = 980$ nm. Figure 3(a) shows the electric field distribution on the xz plane when $y = 0$ nm, and the trapping force along the z direction is presented in Fig. 3(b). We also determined the optical force based on the orthogonal polarization (x direction) of the incident light along the z direction. The optical force at an intensity of 100 mW/μm^2 was in the range of 10^{-2} pN, which is approximately 250 times smaller than that determined using longitudinally polarized incident light (y direction). The x and y positions of the particle are defined by the stable trapping location, obtained from the potential plot in Fig. 4. Positive values of the force, F_z, refer to pulling gradient forces, which attract the particle toward the highest intensity of the local near-field trap, whereas negative values are pushing forces. Figure 3(c) shows the potential, in units of k_BT calculated from the corresponding trapping force, F_z, where k_B is Boltzmann's constant and T is the temperature of the

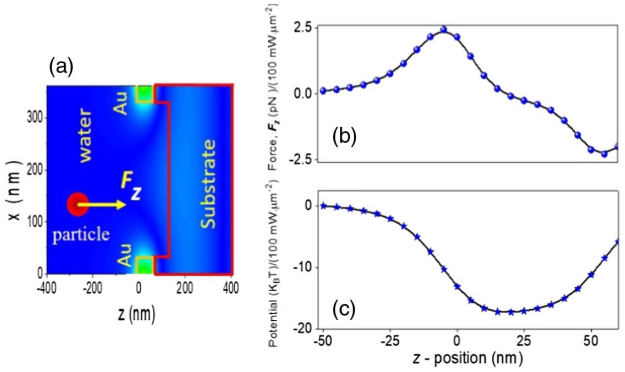

Fig. 3. (a) Electric field distribution for the $y = 0$ plane; (b) trapping force and (c) the corresponding potential curve as a function of particle position along the z direction for $x = 0$ nm and $y = 0$ nm.

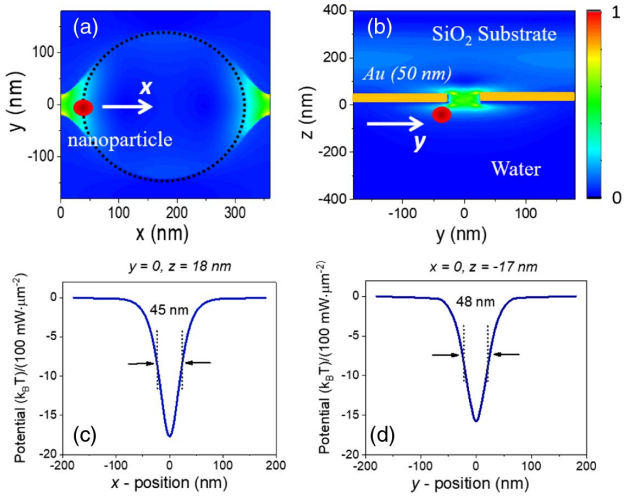

Fig. 4. Electric field distribution on the (a) $z = 18$ nm and (b) $x = 0$ nm planes. Potential plots for a 30 nm particle as a function of the position of the particle along (c) the x direction and (d) the y direction. The sweep directions are shown in (a) and (b) using white arrows for illustration purposes.

Table 1. Simulated and Experimental Trap Stiffness[a]

Wavelength (nm)	k_x (fN/nm)	k_y (fN/nm)	k_z (fN/nm)	Theoretical Stiffness Calculation, k_{tot} (fN/nm)	Experimental Stiffness Measurement, k_{mea} (fN/nm)
980	0.48	0.26	0.50	0.74	0.84 ± 0.25

[a]Theoretical stiffness calculations and experimental observations were normalized to an incident laser intensity of 1 mW/μm^2.

surrounding environment. In principle, a potential well depth of $\sim 10k_BT$ is sufficient to form a stable trap. It is apparent that the hot spot located at the nanoslot forms a stable configuration with a minimal potential depth at $z = 18$ nm due to the repelling and pulling force modulations around the maximum intensity position of the local near field.

The electric field distributions on the xy plane at $z = 18$ nm and the yz plane at $x = 0$ nm are shown in Figs. 4(a) and 4(b), respectively. The potential of the trapped nanoparticle as a function of the x direction is plotted in Fig. 4(c). From the simulated potential results in the x and z directions, the equilibrium position is at $x = 0$ nm and $z = 18$ nm. To obtain the potential profile along the y direction, the nanoparticle was placed 2 nm above the interface between the water and the gold film (i.e., at $x = 0$ nm, $z = -17$ nm), the result of which is shown in Fig. 4(d). The full width at half-maximum (FWHM) for the x and y directions are 45 and 48 nm, respectively. For a particle at a position $r\ (x, y, z)$, by assessing the simulated forces and the FWHM values of the corresponding trapping potentials in Figs. 3 and 4, we calculated the trap stiffness, k_{tot}, using the following standard formula $F = k_{tot} \cdot r$, where $k_{tot} = \{k_x, k_y, k_z\}$ represents the complex component of trap stiffness for the x, y and z directions. The results are shown in Table 1.

3. EXPERIMENTAL RESULTS

For the nanoparticle trapping experiments, a modified Thorlabs optical tweezers kit (OTKB) with an oil immersion objective lens (100×, NA = 1.33) was used. The plasmonic chip was packed in a sample cuvette containing PS particles with a mean diameter of 30 nm (Sigma Aldrich, L5155) [22] in deionized (DI) water with a 0.0625% mass concentration. Detergent Tween 20 with 0.1% volume concentration was used to prevent the formation of clusters. The sample cuvette was mounted and fixed on top of a piezo stage. A Ti:sapphire laser, with wavelength tuned from 940 to 980 nm in 10 nm interval was used for trapping. The FWHM beam size was approximately 1 μm. The number of hot spots that could be excited on the plasmonic array was four, based on the size of the incident laser spot. A 60× objective was used as a condenser to collect the transmitted beam, which was detected by an avalanche photodiode (APD). A data acquisition board (DAQ) was used to record the transmission signal at a frequency of 10 kHz. When a single nanoparticle was trapped in one nanoslot, a clear step increase in transmission was observed. A trace of the raw transmission signal versus time is shown in Fig. 5. The trapping wavelength was 970 nm with 0.57 mW/μm^2 incident power.

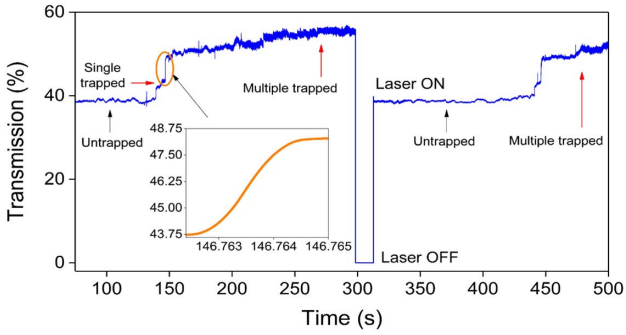

Fig. 5. Raw data trace of transmission signal against time. A zoomed in step increase around the time point of 147.7 s is shown in the inset, which represents a time interval of 0.003 s.

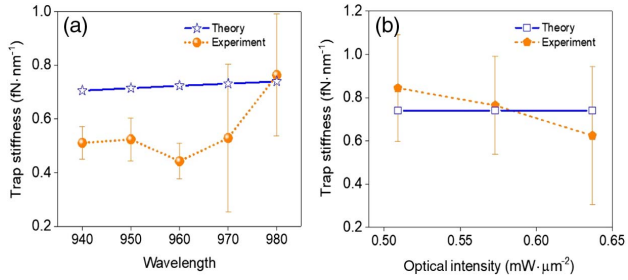

Fig. 6. (a) Trap stiffness for a single 30 nm PS sphere in a near-field trap as a function of wavelength. The experiment was done for an incident laser intensity of 0.57 mW/μm^2. The presented theoretical calculation and experimental observations were normalized to 1 mW/μm^2 laser intensity. Stars, theory; solid circles, experiment; (b) trap stiffness as a function of laser intensity for an incident trapping wavelength of 980 nm. Squares, theory; polygons, experiment.

When multiple particles were trapped by the array, discrete steps in the transmission signal were observed. At around 300 s after the trapping laser was switched on, the beam was blocked to release the trapped nanoparticles. The block was then removed quickly (during about 0.1 s) to demonstrate that nanoparticles were released without the trapping laser beam. The transmission level returned to its initial value when no nanoparticles were trapped. A second trapping experiment with the same trapping laser beam and power was performed by removing the block. A similar trapping performance was observed, with multiple step increases and a higher oscillation amplitude of the transmission signal. High repeatability in trapping was observed.

The transient time for each step in the signal transmission was used to determine the trap stiffness [9]. The motion of a particle as a function of time in an optical trap is described by

$$\frac{\mathrm{d}x(t)}{\mathrm{d}t} = \frac{k_{\mathrm{mea}}}{\gamma}x(t) + \left(\frac{2k_BT}{\gamma}\right)^{1/2}\varsigma(t), \tag{3}$$

where $x(t)$ is the displacement of the particle from its equilibrium position, k_{mea} is the total trap stiffness from a measurement, γ is the Stokes drag coefficient, and $\varsigma(t)$ is white noise. The drag coefficient, γ, and the trapping transient time, τ, are related to k_{mea} from

$$\tau = \frac{\gamma}{k_{\mathrm{mea}}}. \tag{4}$$

By fitting the transient time of a trapping step in transmission, the trap stiffness for a single particle can be calculated.

Table 1 shows the numerically calculated trap stiffnesses, k_x, k_y, k_z, and k_{tot}, where $k_{\mathrm{tot}} = (k_x^2 + k_y^2 + k_z^2)^{1/2}$, and the experimentally measured value of trap stiffness is k_{mea}. Theoretical calculations and experimental observations of the trap stiffness were normalized to an incident laser intensity of 1 mW/μm^2, as shown in Table 1. The experimental value given is the average over multiple runs, with the first four trapping events being included for each run. The error bar is the standard deviation. The highest value of the trap stiffness, 0.844 fN/nm, was observed at 980 nm for 0.51 mW/μm^2 incident intensity. Each trapping event yielded similar values, since the distance between hot spots is large, and we expect there to be no interactions between the trapped particles. The theoretical trap stiffness, k_{tot}, is in reasonable agreement with k_{mea}, with a deviation of approximately 20%. Some of this deviation would be accounted for by the actual size of particles trapped in the experiments (varying from 20 to 40 nm) [22]. When compared to the initial transmission signal with no trapping, the measured step increase in transmission due to the trapping event was 5.89% ± 3.55% for 940 nm and 2.69% ± 1.53% for 980 nm. When compared to simulations, the trend in the experimental data is the same, i.e., the increase in transmission is larger at 940 nm.

Figure 6(a) shows both the experimental and numerical trap stiffnesses for multiple, sequential trapping events of a single ~30 nm PS sphere at a fixed 0.57 mW/μm^2 incident laser intensity for various incident laser wavelengths. The presented data were normalized to 1 mW/μm^2 laser intensity. As expected, the theoretical trap stiffness increases when the trapping wavelength is closer to the resonant value around 980 nm. Experimentally, a similar trend was observed; lower stiffness values were obtained for wavelengths shorter than 970 nm, and the match with the simulations was good for low-intensity trapping at 980 nm. We attribute the large error bars for the trapping lasers at 970 and 980 nm to heating effects, since these two wavelengths are close to resonance. Figure 6(b) shows k_{mea} versus laser intensity at 980 nm. We see that k_{mea} tends to decrease with an increase in laser intensity. The theoretical trap stiffness is also shown in Fig. 6(b). Note that this is constant as a function of the laser intensity, since this parameter is included in the unit of the trap stiffness and we ignore other effects, such as the heating of the gold layer.

4. DISCUSSION

The fabrication of high-quality, plasmonic devices to trap nanoobjects (10–40 nm) at extremely low trapping laser intensities less than 1 mW/μm^2 is now a routine practice in several laboratories. Several studies have demonstrated the possibility of plasmonic optical trapping [18,23]. For example, both trapping and rotation of 110 nm PS beads were achieved using plasmonic nanopillars with an incident light intensity of less than 10 mW/μm^2 [23]. A typical trap stiffness of ~0.1 fN/(nm · mW) for a 10 nm dielectric sphere has been reported [24]. Also, trapping of a single bovine serum albumin

(BSA) molecule with a hydrodynamic radius of 3.4 nm was demonstrated within a plasmonic double nanohole aperture [11,25]. Recently, theoretical studies have shown that optical trapping of particles with sizes less than 10 nm is possible using a hybrid plasmonic coaxial aperture [18] and silicon slot waveguides [26]. A slot photonic crystal cavity that supports multiple modes has also been theoretically investigated, demonstrating a trap stiffness of approximately 3.5 fN/(nm · mW) for 30 nm diameter PS nanoparticles [27].

Here, we optimized the plasmonic nanoslot array in order to perform sequential trapping of single nanoparticles within each individual trapping site. The absorption resonance at 980 nm was chosen for this aim. It is worth mentioning that the design of our plasmonic tweezers array tends to reduce optical interactions between nanoslots. This is a completely different feature from that of periodicity-based plasmonic nanohole array structures [28,29]. Such behavior allows us to distinguish trapped single nanoparticles at different trapping sites with a reasonable stiffness while retaining a low-incident laser intensity. A comparable trap stiffness for sequential particle trapping was experimentally observed within these trapping sites. This confirmed our hypothesis. The applications of this work could include ultrahigh resolution imaging of trapped nano-objects.

For a comparison of trap stiffness between our work and other approaches, we have scaled our measured trap stiffness to that we would expect to obtain for a PS particle with a diameter of 10 nm for an incident laser intensity of 1 $mW/\mu m^2$, since the trap stiffness is proportional to the cubic power of the diameter of the nanoparticle. We also consider Faxén's correction to introduce a factored drag force that arises due to the walls of the nanoslot structure, as previously reported for nanoparticle trapping [30,31]. We assumed that the 30 nm PS particles are trapped 5 nm away from the surface of the plasmonic device's walls and that the Faxén's correction could cause the trap stiffness to increase by a factor of ∼1.78; however, a maximum increase of ∼3.10 can be expected when the particle is touching the wall. Using this maximum correction factor, we thus obtain a scaled trap stiffness of ∼0.1 fN/nm for 10 nm particles. This is comparable to this stiffness of 0.1 fN/nm reported elsewhere [9] and to the numerically predicted stiffness for coaxial aperture trapping of 10 nm PS particles of 0.36 fN/nm [18].

To compare our values of trap stiffness to those for conventional optical tweezers, we used the same scaling method without including Faxén's correction. Our array structure has a total trap stiffness of ∼0.84 fN/nm for a 30 nm dielectric particle; this is about 3 times larger than the total trap stiffness of ∼0.28 fN/nm obtained for a 220 nm particle [32], which is about 7 times larger than the particles we used. Since the stiffness scales as the cubic root of the particle size, our plasmonic tweezer is, therefore, about 1000 times more efficient for nanoparticle trapping than conventional tweezers. We can use much lower laser intensities to achieve trapping as a result.

As we observed in Fig. 6, there is a discrepancy between the numerical and experimental results obtained for the trap stiffness. First, this could be due to the thermal effect when the trapping wavelength approaches the resonance wavelength and the absorption coefficient is approximately 7.9×10^5/cm at 980 nm [33]. The heating effect arising from gold absorption of the light is more severe and can increase the Brownian motion of the trapped particle; this reduces the measured trap stiffness of the plasmonic tweezers. We also obtained large error bars for 970 and 980 nm trapping wavelengths, and this may also be due to thermal effects. It is worth mentioning that, in nonlinear optics, for intense laser irradiation (e.g., laser pulse duration of 120 fs, incident power of 15 mW, and a focused laser beam spot size of 4.5 μm) incident on an aperture, only a 0.1 K increase in temperature has been reported, compared to an 800 K increase for metal nanoparticles [34]. Even though the generation of heat due to the gold film in nanoapertures is small when compared to other LSPP configurations, heating cannot be eliminated at resonant trapping frequencies. Second, the increase in trap stiffness in Fig. 6(b) with decreasing laser intensity is very similar to the self-induced back-action (SIBA) effect. In a resonant SIBA regime, the back-action effect becomes stronger at lower incident trapping powers [35,36]. Apart from these effects, a number of other parameters should be addressed for a complete understanding of the experiment, such as optical torque, interactions between trapped particles, and surface roughness.

We observed that for shorter trapping wavelengths, a longer time was needed for the first trapping event (160 s at 940 nm versus 60 s at 980 nm). This indicates that the volume concentration of the nanoparticles in DI water was low. Due to the effect of Tween 20, which prevents the formation of clusters, the nanoparticles were trapped one by one. In Ref. [25], the authors demonstrated trapping of a single BSA protein by a double nanohole structure, but were unable to observe two BSA proteins trapped at the same site; they concluded that this was due to the physical boundary of the nanostructure. The trapping area of our nanoslot (approximately 44 nm wide in a 50 nm thick gold film) is close to the size of the PS particles used (20–40 nm) [22], and, based on previously mentioned reasons, we conclude that we have trapped single nanoparticles at each trapping site via the plasmonic nanohole array. For trapping wavelengths of 970 and 980 nm, at least four trapping steps were observed, and we attribute this to thermophoresis. Due to heating arising from light absorption by the gold, nanoparticles were brought closer to the hot spots because of the fluid flow. As this is not the focus of the current work, data are not presented.

5. CONCLUSION

We have experimentally demonstrated trapping of single PS nanoparticles using a plasmonic nanohole array. Numerical and experimental values obtained for the trap stiffness were compared, and a reasonable agreement was observed. Note that discrepancies could arise from the 20–40 nm actual size distribution of the particles used in the experiments [22], whereas we assumed a mean diameter of 30 nm particles in all calculations and simulations. The advantage of this plasmonic array over other devices is the possibility it offers to trap nanoparticles with defined separations or in specific patterns. We have done both simulation and experimental work to demonstrate the capability of these arrays in trapping microparticles with extremely low-incident laser intensity [37]. A more precise design of the plasmonic array could be implemented in order to study interactions between trapped particles by adjusting the

spacing between hot spots, and this will be the focus of future work.

Funding. Okinawa Institute of Science and Technology Graduate University.

Acknowledgment. The authors would like to thank S. P. Mekhail and M. Ozer for technical assistance, and M. Sergides and I. Gusachenko for initial contributions to the experimental work.

REFERENCES

1. M. L. Juan, M. Righini, and R. Quidant, "Plasmon nano-optical tweezers," Nat. Photonics **5**, 349–356 (2011).
2. A. Ashkin, J. M. Dziedzic, J. E. Bjorkholm, and S. Chu, "Observation of a single-beam gradient force optical trap for dielectric particles," Opt. Lett. **11**, 288–290 (1986).
3. K. Y. Chen, A. T. Lee, C. C. Hung, J. S. Huang, and Y. T. Yang, "Transport and trapping in two-dimensional nanoscale plasmonic optical lattice," Nano Lett. **13**, 4118–4122 (2013).
4. A. N. Grigorenko, N. W. Roberts, M. R. Dickinson, and Y. Zhang, "Nanometric optical tweezers based on nanostructured substrates," Nat. Photonics **2**, 365–370 (2008).
5. Y. Tanaka and K. Sasaki, "Efficient optical trapping using small arrays of plasmonic nanoblock pairs," Appl. Phys. Lett. **100**, 021102 (2012).
6. B. J. Roxworthy, K. D. Ko, A. Kumar, K. H. Fung, E. K. Chow, G. L. Liu, N. X. Fang, and K. C. Toussaint, Jr., "Application of plasmonic bowtie nanoantenna arrays for optical trapping, stacking, and sorting," Nano Lett. **12**, 796–801 (2012).
7. M. Daly, M. Sergides, and S. Nic Chormaic, "Optical trapping and manipulation of micrometer and submicrometer particles," Laser Photon. Rev. **9**, 309–329 (2015).
8. J. Berthelot, S. S. Acimovic, M. L. Juan, M. P. Kreuzer, J. Renger, and R. Quidant, "Three-dimensional manipulation with scanning near-field optical nanotweezers," Nat. Nanotechnol. **9**, 295–299 (2014).
9. A. Kotnala and R. Gordon, "Quantification of high-efficiency trapping of nanoparticles in a double nanohole optical tweezer," Nano Lett. **14**, 853–856 (2014).
10. Y. Tsuboi, T. Shoji, N. Kitamura, M. Takase, K. Murakoshi, Y. Mizumoto, and H. Ishihara, "Optical trapping of quantum dots based on gap-mode-excitation of localized surface plasmon," J. Phys. Chem. Lett. **1**, 2327–2333 (2010).
11. Y. Pang and R. Gordon, "Optical trapping of a single protein," Nano Lett. **12**, 402–406 (2012).
12. M. Righini, P. Ghenuche, S. Cherukulappurath, V. Myroshnychenko, F. J. G. de Abajo, and R. Quidant, "Nano-optical trapping of Rayleigh particles and *Escherichia coli* bacteria with resonant optical antennas," Nano Lett. **9**, 3387–3391 (2009).
13. O. M. Marago, P. H. Jones, P. G. Gucciardi, G. Volpe, and A. C. Ferrari, "Optical trapping and manipulation of nanostructures," Nat. Nanotechnol. **8**, 807–819 (2013).
14. M. B. Wabuyele and T. Vo-Dinh, "Detection of human immunodeficiency virus type 1 DNA sequence using plasmonics nanoprobes," Anal. Chem. **77**, 7810–7815 (2005).
15. M. Schena, D. Shalon, R. W. Davis, and P. O. Brown, "Quantitative monitoring of gene expression patterns with a complementary DNA microarray," Science **270**, 467–470 (1995).
16. M. A. Cooper, "Optical biosensors in drug discovery," Nat. Rev. Drug Discov. **1**, 515–528 (2002).
17. P. N. Prasad, *Introduction to Biophotonics* (Wiley, 2003).
18. A. A. Saleh and J. A. Dionne, "Toward efficient optical trapping of sub-10-nm particles with coaxial plasmonic apertures," Nano Lett. **12**, 5581–5586 (2012).
19. K. Wang and K. B. Crozier, "Plasmonic trapping with a gold nanopillar," Chem. Phys. Chem. **13**, 2639–2648 (2012).
20. M. Sergides, V. G. Truong, and S. Nic Chormaic, "Highly tunable plasmonic nanoring arrays for nanoparticle manipulation and detection," Nanotechnology **27**, 365301 (2016).
21. F. Hao, E. M. Larsson, T. A. Ali, D. S. Sutherland, and P. Nordlander, "Shedding light on dark plasmons in gold nanorings," Chem. Phys. Lett. **458**, 262–266 (2008).
22. https://www.sigmaaldrich.com/catalog/DataSheetPage.do?brandKey=SIGMA&symbol=L5155.
23. K. Wang, E. Schonbrun, P. Steinvurzel, and K. B. Crozier, "Trapping and rotating nanoparticles using a plasmonic nano-tweezer with an integrated heat sink," Nat. Commun. **2**, 469 (2011).
24. R. A. Jensen, I. C. Huang, O. Chen, J. T. Choy, T. S. Bischof, M. Lončar, and M. G. Bawendi, "Optical trapping and two-photon excitation of colloidal quantum dots using bowtie apertures," ACS Photon. **3**, 423–427 (2016).
25. A. Zehtabi-Oskuie, H. Jiang, B. R. Cyr, D. W. Rennehan, A. A. Al-Balushi, and R. Gordon, "Double nanohole optical trapping: dynamics and protein-antibody co-trapping," Lab Chip **13**, 2563–2568 (2013).
26. A. H. J. Yang, T. Lerdsuchatawanich, and D. Erickson, "Forces and transport velocities for a particle in a slot waveguide," Nano Lett. **9**, 1182–1188 (2009).
27. L. Wang, Y. Cao, T. Zhu, R. Feng, F. Sun, and W. Ding, "Optical trapping of nanoparticles with tunable inter-distance using a multimode slot cavity," Opt. Express **25**, 29761–29768 (2017).
28. C. Genet and T. W. Ebbesen, "Light in tiny holes," Nature **445**, 39–46 (2007).
29. S. Yokogawa, S. P. Burgos, and H. A. Atwater, "Plasmonic color filters for CMOS image sensor applications," Nano Lett. **12**, 4349–4354 (2012).
30. A. J. Goldman, R. G. Cox, and H. Brenner, "Slow viscous motion of a sphere parallel to a plane wall. I. Motion through a quiescent fluid," Chem. Eng. Sci. **22**, 637–651 (1967).
31. J. Happel and H. Brener, *Low Reynolds Number Hydrodynamics: With Special Applications to Particulate Media* (Martinus Nijhoff, 1983).
32. A. Rohrbach, "Stiffness of optical traps: quantitative agreement between experiment and electromagnetic theory," Phys. Rev. Lett. **95**, 168102 (2005).
33. D. I. Yakubovsky, A. V. Arsenin, Y. V. Stebunov, D. Y. Fedyanin, and V. S. Volkov, "Optical constants and structural properties of thin gold films," Opt. Express **25**, 25574–25587 (2017).
34. P. N. Melentiev, A. E. Afanasiev, A. A. Kuzin, A. S. Baturin, and V. I. Balykin, "Giant optical nonlinearity of a single plasmonic nanostructure," Opt. Express **21**, 13896–13905 (2013).
35. P. Mestres, J. Berthelot, S. S. Acimovic, and R. Quidant, "Unraveling the optomechanical nature of plasmonic trapping," Light Sci. Appl. **5**, e16092 (2016).
36. L. Neumeier, R. Quidant, and D. E. Chang, "Self-induced back-action optical trapping in nanophotonic systems," New J. Phys. **17**, 123008 (2015).
37. X. Han, V. G. Truong, and S. Nic Chormaic, "Efficient microparticle trapping with plasmonic annular apertures arrays," Nano Futures **2**, 035007 (2018).

203.181.243.17 {ts '2019-06-12 02:04:39'}